THE JOURNAL OF PHYSICAL CHEMISTRY A
A JOURNAL OF THE AMERICAN CHEMICAL SOCIETY

pubs.acs.org/JPCA Article

Optical Identification of the Resonance-Stabilized *para*-Ethynylbenzyl Radical

Sederra D. Ross, Jonathan Flores, Sima Khani, Daniel M. Hewett, and Neil J. Reilly*

Cite This: *J. Phys. Chem. A* 2021, 125, 9115–9127 Read Online

ACCESS | Metrics & More | Article Recommendations | Supporting Information

ABSTRACT: We report the spectroscopic observation of the jet-cooled *para*-ethynylbenzyl (PEB) radical, a resonance-stabilized isomer of C_9H_7. The radical was produced in a discharge of *p*-ethynyltoluene diluted in argon and probed by resonant two-color two-photon ionization (R2C2PI) spectroscopy. The origin of the $D_0(^2B_1)-D_1(^2B_1)$ transition of PEB appears at 19,506 cm^{-1}. A resonant two-color ion-yield scan reveals an adiabatic ionization energy (AIE) of 7.177(1) eV, which is almost symmetrically bracketed by CBS-QB3 and B3LYP/6-311G++(d,p) calculations. The electronic spectrum exhibits pervasive Fermi resonances, in that most a_1 fundamentals are accompanied by similarly intense overtones or combination bands of non-totally symmetric modes that would carry little intensity in the harmonic approximation. Under the same experimental conditions, the m/z = 115 R2C2PI spectrum of the *p*-ethynyltoluene discharge also exhibits contributions from the *m*-ethynylbenzyl and 1-phenylpropargyl radicals. The former, like PEB, is observed herein for the first time, and its identity is confirmed by measurement and calculation of its AIE and D_0-D_1 origin transition energy; the latter is identified by comparison with its known electronic spectrum (*J. Am. Chem. Soc.*, **2008**, *130*, 3137−3142). Both species are found to co-exist with PEB at levels vastly greater than might be explained by any precursor sample impurity, implying that interconversion of ethynylbenzyl motifs is feasible in energetic environments such as plasmas and flames, wherein resonance-stabilized radicals are persistent.

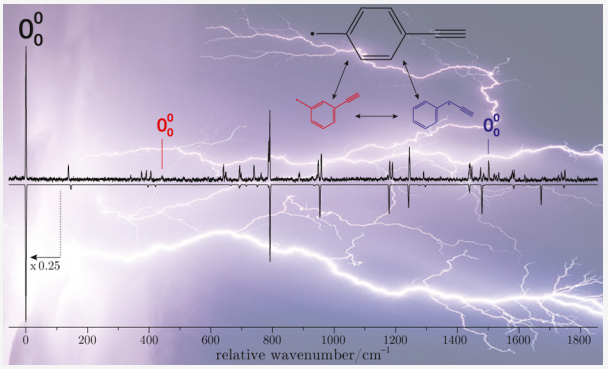

1. INTRODUCTION

The primacy of resonance-stabilized radicals (RSRs) in molecular-weight growth during combustion and pyrolysis is well established. RSRs are the major initial products of unimolecular hydrocarbon decomposition[1,2] because the bonds that must be broken to produce them are relatively weak. For example, thermal decomposition of toluene by way of the delocalized π-radical benzyl is favored over the phenyl and methylphenyl σ-radical channels by *ca.* 90 and 50 kJ mol^{-1}, respectively.[3] This attribute of RSRs, in combination with their relatively slow rates of oxidation and further decomposition, allows their accumulation to high concentrations in flames.[4] The formation of large aromatic species in thermal environments is held to begin with reactions involving the RSRs propargyl (C_3H_3),[5−7] cyclopentadienyl (C_5H_5),[8,9] and benzyl (C_7H_7).[10−12] The recent spectroscopic identification by Johansson and co-workers of specific RSRs desorbed from soot particles[13] points to the extension of radical delocalization over an expanding π-network as a crucial driver of particle inception. Because they are the most stable products formed by the reaction of hydroxyl radicals with unsaturated hydrocarbons,[14−16] it is plausible that RSRs are also important intermediates in tropospheric chemistry. RSRs have furthermore long been implicated in the production of polycyclic aromatic hydrocarbons in stellar outflows,[17−19] and their generally barrierless recombination reactions provide a viable means of synthesizing complex molecules in cold interstellar clouds and planetary atmospheres.[19,20]

The identification of reactive intermediates in complex environments depends critically on the existence of isomer-specific gas-phase spectroscopic data for *in situ* detection. For all but a handful of small unsaturated hydrocarbon systems, theoretical potential energy surfaces exhibit a vastly greater number of intermediates than have been observed in the laboratory.[21−23] As m/z increases, product identification using vacuum ultraviolet photoionization mass spectrometry (VUV-PIMS) can become challenging as multiple isomers with similar ionization potentials may contribute to the photoionization efficiency spectrum. However, further selectivity may be achievable using multiphoton ionization schemes that

Received: August 8, 2021
Revised: September 17, 2021
Published: October 6, 2021

https://doi.org/10.1021/acs.jpca.1c07039
J. Phys. Chem. A 2021, 125, 9115−9127

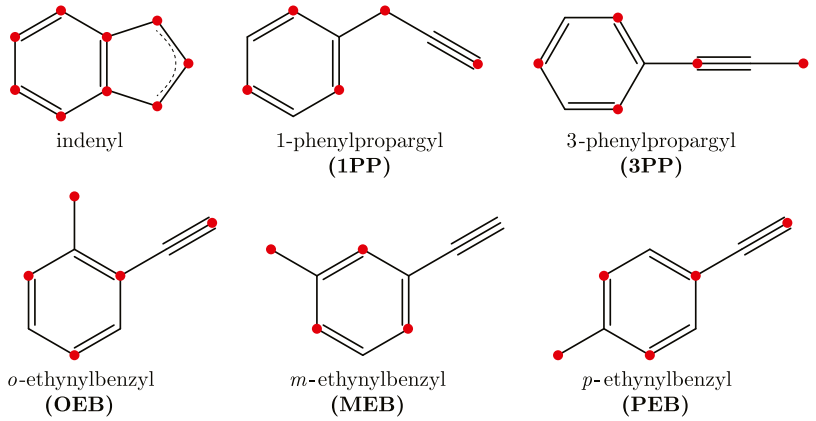

Figure 1. Isomers of C_9H_7 discussed in this work. A red circle indicates the radical site in one of the multiple resonance structures that can be drawn for each isomer. Indenyl, 1-phenylpropargyl (1PP), and 3-phenylpropargyl (3PP) have been spectroscopically observed in the gas phase.[33,34,37]

exploit vibrational[24,25] or optical[26] resonances, particularly under jet-cooled conditions. Indeed, because most RSRs possess low-lying excited electronic states, the optical band has emerged as probably the most fruitful arena for their discovery, particularly in the last couple of decades.[27]

Within this context, we have embarked on optical surveys for new transient species using resonant two-color two-photon ionization (R2C2PI) and laser-induced fluorescence (LIF). We recently reported electronic spectra of previously unobserved resonance-stabilized isomers of C_7H_7 (3-ethynylcyclopentenyl),[28] and much more latterly, C_9H_9 (*cis*- and *trans*-*meta*-vinylbenzyl).[29] The present study concerns isomers with the molecular formula C_9H_7, which appears regularly in the mass spectra of hydrocarbon flames,[30−32] and is highly conspicuous in the soot formation study by Johansson et al.[13] The C_9H_7 potential energy hypersurface has not been well explored spectroscopically, with most gas-phase studies having taken place only in the last 15 years. The global C_9H_7 minimum is the indenyl radical (Figure 1 shows the C_9H_7 RSRs referred to throughout this work). Hemberger and co-workers measured an adiabatic ionization energy (AIE) of 7.53 eV by threshold photoionization spectroscopy.[33] The ground and first excited states of indenyl have been observed by Kim et al. using slow electron velocity-map imaging following electron photodetachment from the anion.[34] The $\tilde{X}$ and $\tilde{A}$ states of indenyl are separated by only ∼0.95 eV and are strongly vibronically coupled,[35] and an $\tilde{A}$-state lifetime of order 10 fs has been inferred from line-broadening.[34] A matrix absorption spectrum near 400 nm has been attributed to indenyl[36] but not yet observed in the gas phase; it may be that higher excited states of indenyl, like the $\tilde{A}$ state, are also too short-lived for observation by action spectroscopies such as LIF and R2C2PI.

Although m/z = 115 signal in hydrocarbon flame assays is usually solely attributed to indenyl,[13,30−32] optical interrogations have revealed the 1PP radical to be a ubiquitous product of hydrocarbon discharges. 1PP was first uncovered in the two-dimensional laser-induced fluorescence spectrum of a dilute benzene discharge, outshone only by intense Swan band transitions of C_2 and the "comet" bands of C_3.[37] The D_0−D_1 transition of 1PP near 476 nm has been studied in detail using LIF and R2C2PI,[38] and higher-lying excited states have been observed using mass-resolved double-resonance techniques.[39] The 3PP isomer lies only 10 kJ mol^{-1} above 1PP[40] but has not yet been observed optically, a possible reason being that whereas 1PP harbors a benzyl-like chromophore, 3PP has more in common with propargyl, and may have a prohibitively short excited-state lifetime. Both phenylpropargyl isomers have been cleanly generated by flash pyrolysis of the parent bromides and examined by threshold photoionization[33,41] and IR-UV double-resonance[24] spectroscopies. The AIEs of 1PP and 3PP differ by maybe 10 meV (7.24 and 7.25 eV, respectively); as such, the two isomers should be distinguishable from indenyl by VUV-PIMS, provided the relevant photon energies are accessible, but probably not from each other.[41]

The *ortho*-, *meta*-, and *para*-ethynylbenzyl (PEB) radicals, of which the last is perhaps the most stable, are another 20−30 kJ mol^{-1} above 1PP (which one might also call α-ethynylbenzyl) and thus *ca.* 150−160 kJ mol^{-1} less stable than indenyl.[42,43] It is conceivable that the ethynylbenzyls may be produced by barrierless addition of the CH radical to phenylacetylene,[44−46] rendering them species of possible interest to combustion and astrochemistry. All three radicals should be substantially resonance-stabilized—not less than benzyl, and perhaps more so in the case of the ortho and para isomers—and therefore able to survive in energetic environments. To the best of our knowledge, no gas-phase investigation of ethynylbenzyl has been reported,[47] which is surprising in view of the existing vast spectroscopic literature on substituted benzyl systems.[27] More generally, beyond a handful of largely preliminary studies of the isoelectronic cyanobenzyl radicals[48−51] and our own very recent report on *m*-vinylbenzyl,[29] apparently no attention has been devoted to benzyl radicals bearing a ring substituent that extends π-conjugation.

Herein, we describe the D_0−D_1 optical transition of PEB. Pervasive anharmonic resonances are apparent, in that two or more features of similar intensity are observed in almost every instance where the harmonic approximation would admit a single conspicuous a_1 fundamental. Vibronic intensity-borrowing effects are important to consider for some assignments, but not nearly to the pathological extent of the benzyl 454.5 nm transition.[52,53] The 1PP and *m*-ethynylbenzyl (MEB) radicals are conclusively identified under the same experimental conditions, the latter species also for the first time. Prompted by similar observations for the xylyl systems,[45,54] we discuss the implications of these results in terms of possible unimolecular rearrangements among C_9H_7 isomers.

https://doi.org/10.1021/acs.jpca.1c07039
J. Phys. Chem. A 2021, 125, 9115−9127

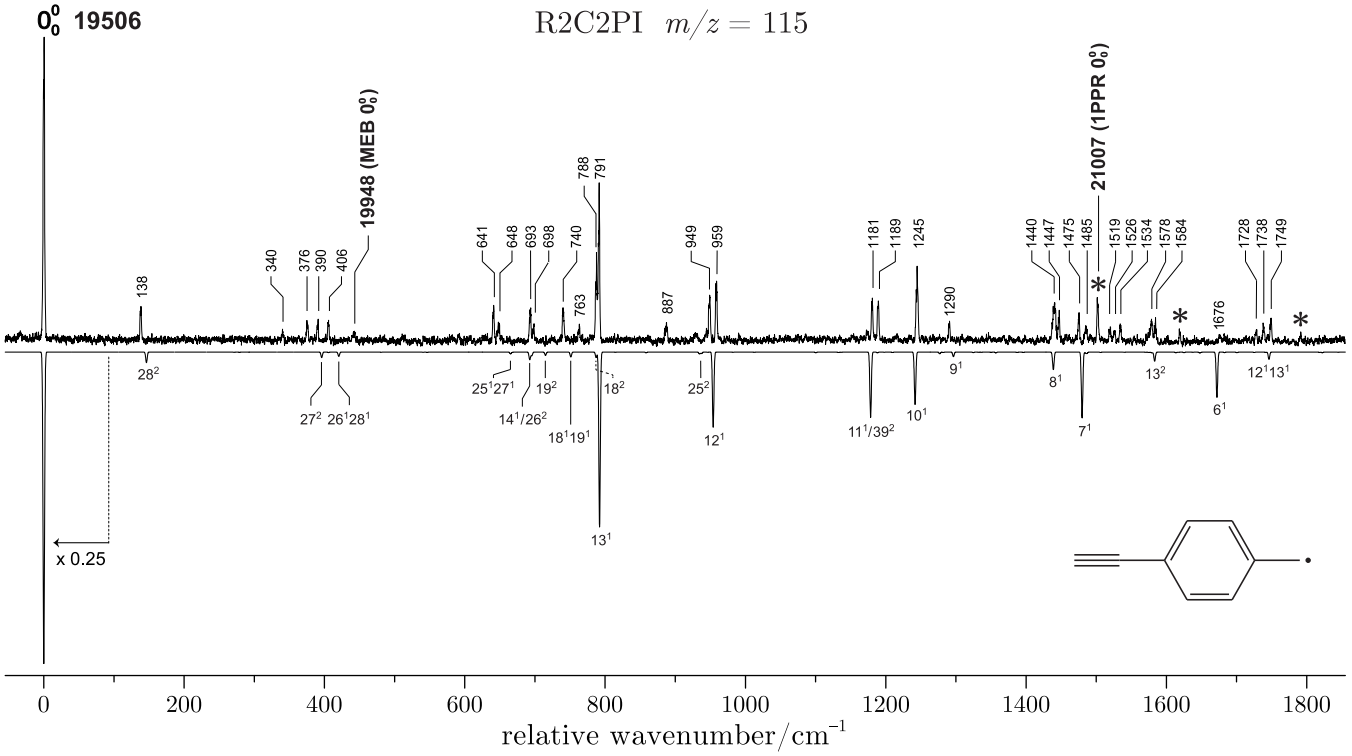

Figure 2. R2C2PI spectrum of the jet-cooled PEB radical, produced in a discharge of *p*-ethynyltoluene diluted in Ar. The reflected trace is a FC simulation. Band positions are reported relative to the PEB D_0-D_1 origin at 19,506 cm^{-1}. The feature at 19,948 cm^{-1} is assigned as the MEB D_0-D_1 origin, and transitions of 1PP[37] are indicated with asterisks (see Section 4.4). Assignments are given in Table 2; see Section 4.3 for further discussion for further discussion.

2. EXPERIMENTAL SECTION

The vacuum chamber used for R2C2PI experiments has been described previously.[28,45] The precursor, *p*-ethynyltoluene, was stored at room temperature in a stainless-steel reservoir and entrained in Ar at 3 atm, admitting a seed ratio smaller than 0.1%. *para*-Ethynylbenzyl (PEB) was generated using a pulsed discharge nozzle,[55] consisting of annular copper electrodes and Vespel insulators mounted to the faceplate of a pulsed solenoid valve with 0.5 mm orifice. The discharge pulse (800 V, 50 μs) was delivered through a current-limiting 50 kΩ resistance as the gas pulse (*ca.* 300 μs duration) traversed the ~10 mm long region between the electrodes. Cooling of the products to a rotational temperature of roughly 10 K and a similar or lower vibrational temperature was achieved by supersonic expansion into vacuum. The base pressure in the source region was 1×10^{-7} Torr, rising to *ca.* 3×10^{-5} Torr with the nozzle operating at 10 Hz.

The central part of the expansion passed through a 2 mm skimmer into the extraction region of a time-of-flight mass spectrometer. The skimmed beam was exposed to visible radiation from a Nd:YAG-pumped pulsed dye laser (520−460 nm using Coumarin 460, 480, and 500 dyes pumped at 355 nm; tunable output of 5 mJ/pulse, 8 ns pulse duration, and 0.2 cm^{-1} linewidth), followed *ca.* 5−10 ns afterward by UV radiation (1 mJ/pulse, 8 ns duration) generated by frequency-doubling the fundamental output of a second 355 nm-pumped pulsed dye laser containing Coumarin 460 dye. The visible beam was propagated orthogonal to both the molecular beam and the UV beam, with the latter directed into the throat of the nozzle. Radicals having transitions resonant with the visible beam were ionized by the UV beam, extracted into a 1 m field-free drift tube, and detected with a tandem microchannel plate. The signal was passed to an oscilloscope, averaged for 64 shots, and transferred to a PC for processing. The m/z = 115 channel was integrated as a function of the visible wavelength, yielding the electronic excitation spectrum. During excitation scans, the wavelength of the UV beam (225 nm) was chosen to avoid dissociative multiphoton ionization of the precursor, which could otherwise pollute the m/z = 115 channel. AIE measurements were then carried out by fixing the visible wavelength to a putative origin transition and scanning the UV beam through the ionization threshold. The wavelengths of both dye lasers were calibrated using a wavemeter of absolute accuracy 0.2 cm^{-1}. All pulsed instruments were triggered at 10 Hz with digital delay generators.

3. COMPUTATIONAL DETAILS

Density functional theory (DFT) calculations were carried out using the Gaussian 09 package.[56] Equilibrium geometries and harmonic vibrational frequencies of the ground (DFT) and first excited states (TDDFT) of neutral ethynylbenzyl radicals, and their cation S_0 states, were calculated with the B3LYP functional and 6-311G++(d,p) basis. Because experimental AIEs of RSRs are generally *ca.* 0.1 eV higher (respectively, lower) than those predicted by B3LYP/6-311G++(d,p)[40] (respectively, CBS-QB3[28]) calculations, the latter method was also applied to neutral and cationic ground states for the purposes of bracketing AIEs. Franck−Condon (FC) factors for the D_0-D_1 transition of PEB were calculated using the FCLab II program of Pugliesi and co-workers,[57,58] which accounts for the effects of normal coordinate (i.e., Duschinsky) rotation; it does not include treatment of Herzberg−Teller effects. In the FC simulation, excited-state vibrational frequencies were scaled

https://doi.org/10.1021/acs.jpca.1c07039
J. Phys. Chem. A 2021, 125, 9115−9127

by 0.976, which factor is in good agreement with experiment for totally symmetric vibrations. The PEB origin rotational contour was simulated with PGOPHER,[59] using rotational constants taken from the optimized D_0 and D_1 geometries.

4. RESULTS AND DISCUSSION

4.1. Identification of *p*-Ethynylbenzyl. Figure 2 shows the R2C2PI spectrum recorded for the m/z = 115 products of the *p*-ethynyltoluene discharge in the region 19,450−20,350 cm^{-1} (roughly 514−469 nm); the reflected trace is a FC simulation. PEB belongs to the C_{2v} point group in its D_0 and D_1 electronic states, and its 42 normal modes are divided into four irreducible representations comprising $15a_1 + 4a_2 + 9b_1 + 14b_2$ vibrations. Table 1 contains all D_0 and D_1 unscaled harmonic vibrational frequencies from B3LYP computations. We herein identify the principal inertial axes *a*, *b*, and *c* with the Cartesian axes *z*, *y*, and *x*, respectively. Symmetry species b_2 and b_1 correspond to in-plane and out-of-plane, respectively; π-molecular orbitals transform as b_1 or a_2. The D_0−D_1 transition is polarized along the molecular *a*-axis and is assigned as $^2B_1$−$^2B_1$. The FC simulation incorporates all transitions into levels involving up to four quanta in four modes, such that the overall vibrational symmetry in D_1 is a_1. Vibrational assignments are presented in Table 2; their detailed justification is deferred until Section 4.3. The observed spectrum might be partially saturated; the origin may thus be somewhat more dominant than measurement implies, as is quite typical in aromatic RSR chromophores (see, e.g., refs 37, 60−62).

Our discovery of PEB was serendipitous: during surveys for the related *p*-vinylbenzyl radical (C_9H_9) in the *p*-vinyltoluene discharge, we observed no resonant signal in the m/z = 117 channel but found a conspicuous product at m/z = 115. A roughly 5-fold increase in the signal-to-noise ratio at 19,506 cm^{-1} was observed using *p*-ethynyltoluene as the precursor, strongly implicating PEB as the carrier. This diagnosis was confirmed by fixing the visible beam to 19,506 cm^{-1} and monitoring the appearance of ions at m/z = 115 as the UV beam was scanned (Figure 3). A threshold two-color appearance potential (2CAP) of 7.177(1) eV is observed, which figure includes an additional 10 meV correction to account for the static field in the ToF spectrometer. The quoted uncertainty derives mainly from two sources: uncertainty in the observed threshold, which is determined from the intersection of straight lines fit to the baseline and to the onset of two-color ion signal (as, e.g., in ref 63), and is generously estimated as 7×10^{-4} eV; and uncertainty associated with the field correction, which we estimate as 3×10^{-4} eV for a field of 240 V cm^{-1} from characterization on other radicals in our laboratory. The sum in quadrature is of order 8×10^{-4} eV and is conservatively rounded to 1 meV. The quite abrupt onset, as shown in Figure 3, implies a significant overlap of the wavefunctions of the neutral D_1 and cation S_0 zero-point levels, and thus that the 2CAP represents the D_0−S_0 AIE. Table 3 contains spectroscopic properties relevant for the identification of ethynylbenzyl radicals. CBS-QB3 and B3LYP/6-311G++(d,p) calculations for PEB yield predictions of 7.25 and 7.08 eV for the AIE, respectively, almost symmetrically bracketing observation. These two methods tend to over/undershoot experiment by roughly 0.1 eV,[28] respectively.

The calculated PEB origin transition energy agrees tolerably well with experiment, given the level of theory. That the transition appears to the red of the benzyl origin (22,002 cm^{-1}) can be rationalized from simple Hückel considerations. Five canonical Lewis structures can be drawn for PEB: four of them correspond with resonance forms of benzyl, and a fifth has the unpaired electron on the ethynyl terminus, implicating the ethynyl group in the chromophore. The second-highest occupied molecular orbital (SHOMO) and the lowest unoccupied molecular orbitals (LUMO) of benzyl transform as a_2 and have energies of β and $-\beta$ with respect to the HOMO (β being the resonance integral). In PEB, the SHOMO and LUMO are of b_1 symmetry, having predominantly ethynyl bonding and anti-bonding character, respectively, and lying modestly (*ca.* 0.19β) above and below the a_2 orbitals, implying a red-shifted absorption, as observed. The

Table 1. All Unscaled B3LYP/6-311++G(d,p) Harmonic Frequencies (cm^{-1}) of PEB Radical in the Ground (D_0) and First Excited (D_1) States[a]

mode	symmetry	D_0	D_1
1	a_1	3475	3463
2		3191	3195
3		3168	3168
4		3145	3155
5		2171	2008
6		1592	1714
7		1511	1517
8		1492	1475
9		1302	1329
10		1236	1273
11		1165	1208
12		1011	978
13		836	812
14		716	710
15		422	416
16	a_2	974	963
17		821	762
18		528	403
19		388	366
20	b_1	967	963
21		841	805
22		762	716
23		719	654
24		619	153
25		535	479
26		418	356
27		231	203
28		95	75
29	b_2	3241	3253
30		3190	3193
31		3167	3166
32		1526	1386
33		1455	1511
34		1335	1248
35		1299	1308
36		1144	1123
37		975	959
38		694	657
39		650	620
40		540	542
41		355	350
42		149	143

[a]Displacement vectors for modes assigned or discussed in the text are presented in Supporting Information, Figure S7.

https://doi.org/10.1021/acs.jpca.1c07039
J. Phys. Chem. A 2021, 125, 9115−9127

Table 2. Assignments for the R2C2PI Spectrum of PEB Radical[a]

exp.	calc.	assignment	exp.	calc.	assignment
0	0	0_0^0	1181	1178	11_0^1
138	146	28_0^2	1189	1210	39_0^2
340		?	1245	1242	$10_0^1/20_0^1 26_0^1$
376	396	27_0^2	1290	1296	9_0^1
390	420	$26_0^1 28_0^1$	1440	1457	$[13_0^1 25_0^1 27_0^1]$
406	406	15_0^1	1447	1439	8_0^1
641	696	$[26_0^2]$	1475	1480	7_0^1
648	665	$[25_0^1 27_0^1]$	1485	1484	$13_0^1 14_0^1$
693	693	14_0^1	1519	1487	$[17_0^2]$
698	715	19_0^2	1526	1538	$18_0^3 19_0^1$
740	751	$18_0^1 19_0^1$	1534	1543	$13_0^1 18_0^1 19_0^1$
763	840	$[26_0^2 28_0^2]$	1578	1579	$13_0^1 18_0^2$
788	787	18_0^2	1584	1584	13_0^2
791	792	13_0^1	1676	1672	$[6_0^1]$
887	935	$[25_0^2]$	1728	1722	$18_0^2 23_0^1 26_0^1$
949	985	$23_0^1 26_0^1$	1738	1727	$13_0^1 23_0^1 26_0^1$
959	954	12_0^1	1749	1746	$12_0^1 13_0^1$

[a]Band positions are reported relative to the origin at 19,506 cm^{-1}. Tentative assignments are enclosed by square brackets; "?" denotes an unknown assignment. Calculated (TDB3LYP/6-311G++(d,p)) frequencies have been scaled by 0.976, which yields optimal agreement for a_1 modes.

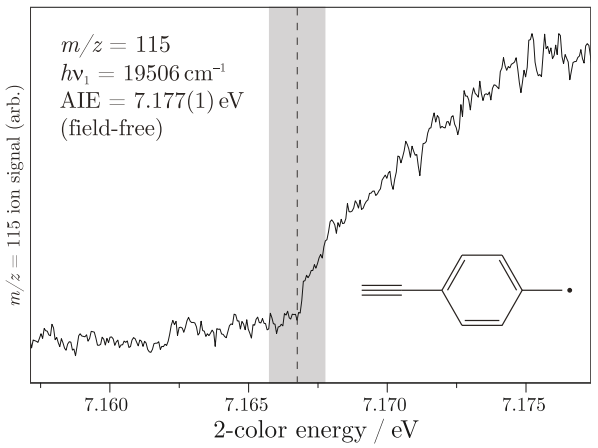

Figure 3. Mass-selected two-color ion-yield scan of PEB radical, measured *via* its D_0-D_1 origin at 19,506 cm^{-1}. The shaded region represents a conservative uncertainty of 1 meV (see the text for explanation). The field-free AIE (7.177(1) eV) exceeds the observed threshold by 10 meV.

size of the shift (454.5 nm for benzyl to 512.6 nm for PEB) is consistent with an empirical rule-of-thumb that has emerged for delocalized π-chromophores, *viz.*, that extension by a C_2 unit red-shifts the absorption wavelength by roughly 60 nm.[27]

There is no doubt that other C_9H_7 isomers contribute to the R2C2PI spectrum. The minimum two-color energy used in excitation scans was roughly 7.85 eV; this is well above the known AIE of 1PP (~7.24 eV[26,41]), which has its D_0-D_1 origin at 21,007 cm^{-1} (2.605 eV; 476.03 nm).[37] The two-color energy should also have permitted ionization of the other ethynylbenzyl radicals; their optical spectra are not known, but their appearance nearby would not be entirely surprising given their predicted transition energies (Table 3). The identification of other isomers and their possible interconversion in the discharge are discussed further in Section 4.4.

Table 3. Calculated and Observed Spectroscopic Properties of Ethynylbenzyl Radicals: Adiabatic Ionization Energies (AIE; eV), D_0-D_1 Adiabatic Transition Energies (T_0; eV), and Vertical Oscillator Strengths ($f_{A\leftarrow X}$)[a]

property	PEB	MEB	OEB
calculated AIE	7.25*/7.08	7.37*/7.28	7.28*/7.15
observed AIE[b]	7.177(1)	7.332(2)	
calculated T_0	2.59	2.55	2.44
observed T_0	2.42	2.47	
$f_{A\leftarrow X}$	0.0102	0.0001	0.0027

[a]Asterisks denote properties from CBS-QB3 calculations; all other computed quantities derive from B3LYP/6-311G++(d,p) calculations. B3LYP energies include ZPE. [b]The observed AIEs include a +0.01 eV empirical correction to account for the static electric field (240 V/cm) in the ToF mass spectrometer.

4.2. Overview of the D_0-D_1 Transition. PEB is an odd-alternant π-system. As such, its Hückel π-MOs occur in pairs that lie exactly astride the zero level (α) and differ in sign for every other atomic orbital coefficient.[64] In such systems, the configurations arising from SHOMO−HOMO and HOMO−LUMO excitations interact to bring about a D_1-D_0 transition that is typically weak and appears in the optical band[65] (*cf.* Table 3). The frontier orbitals (SHOMO, HOMO, and LUMO) of PEB transform as b_1; the D_0-D_1 transition is thus assigned as $^2B_1-^2B_1$ and is polarized along the *a*-axis. A rigid asymmetric top Hamiltonian simulation (with PGOPHER[59]) of the origin rotational contour, using B3LYP D_0 and D_1 geometries and assuming an *a*-type transition, accords well with experiment (Figure 4). The simulation indicates that the rotational temperature of PEB in the molecular beam is close to 7 K.

The optimized D_0 and D_1 structures are shown in Figure 5. The major changes in geometry can be understood by inspection of the frontier π-orbitals (Supporting Information, Figure S1). The SHOMO and LUMO have significant bonding and antibonding character, respectively, for C4−C5/C5−C6 and C5′−C6′ (and similarly, but to a lesser extent, for

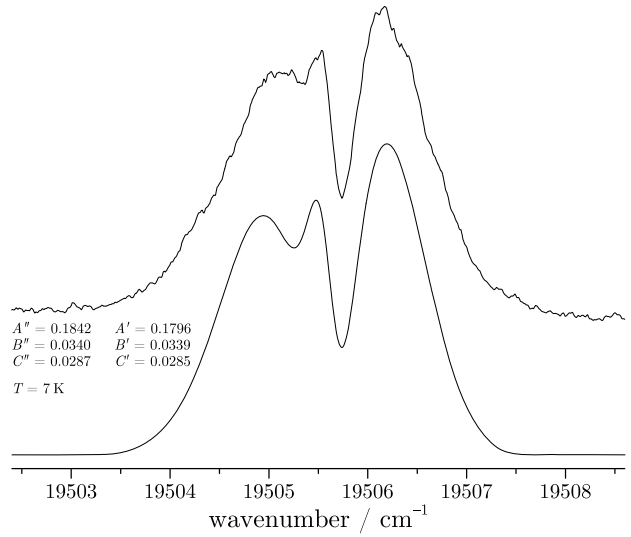

Figure 4. Profile of the R2C2PI 19,506 cm^{-1} band and a simulated rotational envelope at 7 K carried out with PGOPHER,[59] using PEB rotational constants from B3LYP/6-311++G(d,p) calculations. An *a*-type transition is assumed.

https://doi.org/10.1021/acs.jpca.1c07039
J. Phys. Chem. A 2021, 125, 9115−9127

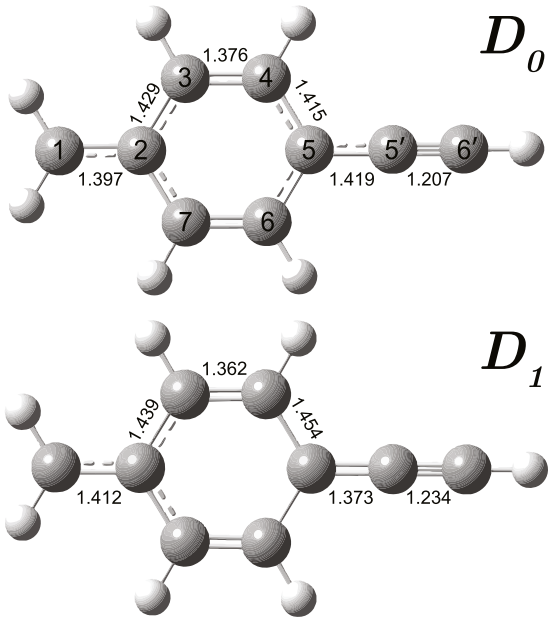

Figure 5. Optimized geometries of the ground (D_0) and first excited (D_1) states of PEB radical from B3LYP/TD-B3LYP calculations with 6-311G++(d,p) basis. Complete Cartesian coordinates are given in the Supporting Information.

C1−C2 and C2−C3/C2−C7), which bonds are thus modestly (*ca.* 0.01−0.03 Å) lengthened by one-electron excitations into and out of the predominantly non-bonding HOMO. Essentially, the reverse is true for C5−C5′ and C3−C4/C7−C6, which contract (by roughly 0.015−0.045 Å) upon excitation. Changes in the bond angle are largely negligible (generally less than a few tenths of a degree): the biggest difference involves ∠C4C5C6, which is 1.3° smaller in D_1. There is no restriction on Δv for a_1 modes, but transitions with $\Delta v > 1$ are weak in large RSRs because structural changes are delocalized over an extended chromophore; usually, no coordinate is singularly affected. The point group of PEB is C_{2v} in both electronic states, meaning that there are no displacements along nontotally symmetric modes. In the zero approximation, Δv must be even for such modes, and their FC activity is governed by the (generally small) changes in their force constants.

One might therefore expect an origin-dominated electronic spectrum with modest off-diagonal activity among totally symmetric distortions of the carbon skeleton. This view is in large part borne out by observation, but there are three significant qualitative departures. One, the intensities of 15_0^1 and 14_0^1 are significantly underestimated (almost to the point of absence), and the dominance of the origin significantly overestimated, in the FC approximation. This could partly—but probably not entirely—be a consequence of saturation, as implied in Section 4.1. Two, several transitions of the type $X_0^1Y_0^1$ have been identified, where X and Y are nontotally symmetric modes of the same symmetry species. Such transitions are forbidden in the zero (i.e., parallel double harmonic) approximation since both integrals in the product $\langle X^1|0''\rangle\langle Y^1|0''\rangle$ are necessarily zero. Three, and most striking: where the FC simulation implies a conspicuous a_1 fundamental, the observed spectrum exhibits two or more closely spaced bands of similar intensity. Notable examples include the features at 788/791; 949/959; 1181/1189; 1245 cm^{-1} (which, being ∼40% broader than most bands, must comprise at least two transitions); and 1440/1447 cm^{-1}. These three major discrepancies principally arise, respectively, from Herzberg−Teller coupling, Duschinsky rotation, and Fermi resonance, which we discuss in turn.

4.2.1. Herzberg−Teller Coupling. It is often the case that the low-lying electronic states of benzyl chromophores are mixed by in-plane vibrations, benzyl itself representing a well-studied and perhaps pathological example.[52,53,66,67] If the product symmetry $\Gamma^{\tilde{A}}_{elec}\otimes\Gamma_Q$ for some vibrational coordinate Q contains the irreducible representation of a nearby bright state, the $\tilde{A} \leftarrow \tilde{X}$ transition may acquire dipole intensity from that state *via* distortion along Q. Table 4 shows vertical TDB3LYP

Table 4. TD-BLYP/6-311G++(d,p) Electronic States, Vertical Transition Energies (eV), and Oscillator Strengths (f) of PEB

state	ΔE	f
$\tilde{X}^2B_1$ (D_0)	0	
$\tilde{A}^2B_1$ (D_1)	2.82	0.0102
1^2A_2	3.15	0.0010
2^2A_2	3.76	0.0261
1^2B_2	3.89	0.0000
1^2B_1	4.12	0.5128
1^2A_1	4.34	0.0005

energies and oscillator strengths for several excited states of PEB. Lending states must be of symmetry A_1, A_2, or B_1; excitation to vibronic states of B_2 symmetry from the B_1 ground state is dipole-forbidden. Intensity-borrowing through b_1 modes is probably negligible as the nearest A_1 state is relatively distant in energy and carries little oscillator strength. The D_1 (or $\tilde{A}$-) state may mix with the 1^2A_2 and 2^2A_2 states through b_2 vibrations, but only the latter, having the larger f-value, might be a significant source of transition moment. It is, for example, a distant possibility that the weak feature at 340 cm^{-1}, which resists even tentative assignment (perhaps because it arises from another species; *vide infra*), could be assigned as 41_0^1. A b-type transition would consequently be expected but cannot be discerned from the 340 cm^{-1} band profile at the present signal-to-noise ratio. On the whole, vibronic coupling *via* b_2 vibrations should be much less significant in PEB than it is in benzyl and the isoelectronic p-cyanobenzyl radical, in which both have relatively closely spaced B_1 and A_2 states with widely disparate oscillator strengths.[48,52,53,68]

More important is the 2^2B_1 state—the brightest by more than an order of magnitude. This state can be described as deriving from the symmetric combination of SHOMO−HOMO and HOMO−LUMO excitations (the D_1 state represents the antisymmetric combination and suffers destructive transition moment interference). It can lend oscillator strength to the $\tilde{A}$-state (1^2B_1) through a_1 vibrations. Precisely this mechanism in the electronic spectrum of benzyl is held responsible for the anomalously large intensity of $6a_0^1$ (13_0^1 in Mulliken notation), whereby the 1^2A_2 state is endowed with the character of its much brighter 3^2A_2 counterpart,[52,53,66] lying ∼1 eV higher in energy. When a totally symmetric mode a is HT (Herzberg Teller)-active, as well as FC-active due to displacement along Q_a, the intensity of every transition is affected because the term $\frac{\partial\mu}{\partial Q_a}\langle 0'_a|Q_a|0''_a\rangle$ must be non-zero; however, the effect is most consequential when HT-active

https://doi.org/10.1021/acs.jpca.1c07039
J. Phys. Chem. A 2021, 125, 9115−9127

modes are excited explicitly. In the *a*-type S_0-S_1 transition of the closely related phenylacetylene molecule, for example, inclusion of Herzberg–Teller moments up to second order is necessary to explain the prominence of several a_1 fundamentals, whereas at the Condon level the spectrum is wrongly predicted to be strongly origin-dominated.[69] In the present case, TDB3LYP calculations for displacements $Q-Q_0$ along several a_1 modes generally evince strong modulation of the *z*-polarized PEB D_0-D_1 transition moment (Supporting Information, Figure S2), necessarily (by symmetry) owing to mixing with the 2^2B_1 state.

4.2.2. Duschinsky Rotation. For small displacements, it is valid to relate ground- and excited-state normal coordinates $\mathbf{Q}''$ and $\mathbf{Q}'$ according to a shift vector $\mathbf{K}$ and a rotation (Duschinsky) matrix $\mathbf{J}$, *viz.*, $\mathbf{Q}' = \mathbf{J}\mathbf{Q}'' + \mathbf{K}$.[70] For PEB, elements of $\mathbf{K}$ are only non-zero for a_1 modes, and $\mathbf{J}$ is block-diagonal in the symmetry species. Within the a_1 and b_2 blocks, our calculations suggest no significant rotation (i.e., off-diagonal elements are negligible) for modes with frequencies below 1200 cm^{-1}. The b_1 and a_2 blocks (Supporting Information, Figure S3), however, show substantial rotation among several relatively low-frequency modes, particularly 18 and 19. Such mixing allows combination bands $X_0^nY_0^m$, *n*, *m* odd, where *X* and *Y* are nontotally symmetric modes of the same irreducible representation. The FC factors for the simulation, as shown in Figure 2, were calculated with the FCLab II program[57,58] using the recursion relations of Doktorov,[71] which account for Duschinsky rotation.

4.2.3. Fermi Resonance. For a majority of transitions assigned as a_1 fundamentals, a consort of similar intensity can be found within roughly 10 cm^{-1} and assigned as either an overtone or combination band in one or more nontotally symmetric modes. Since most vibrational frequencies are predicted to change by less than 10% upon excitation, the strength of these features is vastly greater than expected on FC premises. Second-order Herzberg–Teller moments are a possible cause, but the simpler and more plausible explanation is Fermi resonance. If it so happens, for a totally symmetric mode *A* and nontotally symmetric modes *X* and *Y* of the same irreducible representation, that $\omega_A \approx 2\omega_X$ or $\omega_A \approx \omega_X + \omega_Y$, then the levels A^1 and X^2, or A^1 and X^1Y^1, may be coupled through cubic potential terms containing $Q_AQ_X^2$ or $Q_AQ_XQ_Y$, respectively. The intensity associated with the zero-order bright state A^1 is fractionated over the mixed eigenstates; both contain A^1 character (this implies that the excitation spectrum would be significantly less origin-dominated in the absence of Fermi resonance, further suggesting HT enhancement of a_1 fundamentals). In such instances, modes *X* and *Y* need not be Duschinsky-mixed to allow "$X_0^1Y_0^1$" since its intensity derives from the fully allowed A_0^1 contribution.

If only two zero-order states are coupled, the perturbed levels and eigenstates may be obtained by diagonalization of the effective Hamiltonian matrix

$$\begin{pmatrix} 0 & V \\ V & \Delta E \end{pmatrix}$$

where ΔE is the energy difference between the uncoupled levels and *V* is their coupling matrix element. For each of the putative Fermi doublets at 949/959, 1181/1189, and 1440/1447 cm^{-1}, the closely similar intensities of the two components imply that ΔE is small relative to *V* (of order 0.5 cm^{-1} or smaller), with *V* roughly equal to half of the observed splitting (3–5 cm^{-1}). For the features at 788/791, with intensities in the approximate ratio 1:2, ΔE and *V* are more similar—of order 1 and 1.5 cm^{-1}, respectively. It is assumed in each case that all of the zero-order intensity is carried by the a_1 mode, which the FC simulation implies is a reasonable approximation. More thorough analyses can be performed if the emission intensities from each Fermi component to the analogous ground-state levels are known, since a correct description of both excitation and emission intensities is sensitive to small changes in ΔE and *V*,[72,73] and may be complicated further by resonances among ground-state levels. To this end, single vibronic level emission (SVLE) spectroscopy is currently being undertaken in our laboratory.

4.3. Detailed Assignments. With the above considerations borne in mind, we focus now on the assignments that require detailed commentary. There can be little argument that 138 cm^{-1} = 28_0^2, yielding $\nu'_{28} \approx 70$ cm^{-1}, which we use in assigning combination bands. The region 0_0^0 + 340–450 cm^{-1} contains five bands where the FC simulation indicates only two. The 19,948 cm^{-1} band owes to MEB, as shown in Section 4.4. The feature at 340 cm^{-1} is puzzling and may belong to another isomer—perhaps *ortho*-ethynylbenzyl. We have also observed PEB by laser-induced fluorescence (Supporting Information, Figuer S4), and while there is a mostly one-to-one correspondence between REMPI and LIF, there is no obvious band at 340 cm^{-1} in the fluorescence spectrum (perhaps, we concede, because the LIF signal-to-noise ratio is relatively low). Nor, if PEB is its carrier, does it have an obvious assignment. The calculated PEB D_1 frequencies suggest five possibilities—27_0^2, 42_0^2, 41_0^1, $24_0^127_0^1$, or 24_0^2—but none is particularly convincing. The first two assignments would require egregious disagreement (*ca.* 20%) between theory and experiment for ν'_{27} or ν'_{42}; moreover, the former mode can be implicated in more plausible assignments, and the latter should be largely FC-inactive. The third suggestion would involve a vibronically induced transition in a b_2 mode, but the most likely lending state, 2^2A_2, is neither particularly close in energy nor vastly brighter than D_1.

Concerning the last two alternatives, the D_1 frequency for mode 24, the out-of-plane ethynyl hydrogen bend, is highly uncertain. Predictions for ν_{24} in D_0 using various functionals are not grossly dissimilar, ranging from 620 cm^{-1} (B3LYP) to 687 cm^{-1} (M06-2x); however, calculated D_1 values vary by a factor of nearly three, from 153 cm^{-1} (B3LYP) to 434 cm^{-1} (M06-2x). No other mode shows such sensitivity to the choice of functional in either state. If the lower frequency (153 cm^{-1}) was accurate, the implied ~fourfold diminution in ν_{24} would cause significant intensity in both $24_0^127_0^1$ (because of predicted Duschinsky rotation with mode 27) and 24_0^2, but this does not even qualitatively agree with observation. We have thus omitted mode 24 transitions from the FC simulation as their frequencies and intensities are likely misleading. The out-of-plane C≡CH bend is similarly troublesome in other ethynyl-bearing RSR chromophores. The 2^2B_1 state of propargyl has a double minimum in the ∠CCH coordinate,[74,75] and attempts have been made to assign the propargyl $1^2B_1-2^2B_1$ transition in terms of C_{2v}[75] and C_s selection rules.[76] Similarly, the first A'' excited state of the 1-vinylpropargyl chromophore appears to harbor a ∠CCH double minimum,[28,77] presumably owing to the interaction with a nearby A' state *via* the a'' CCH bend. A relatively sophisticated vibronic coupling calculation may therefore be necessary for accurate vibrational intervals in D_1, but the B3LYP harmonic D_0 frequency may be sufficiently

https://doi.org/10.1021/acs.jpca.1c07039
J. Phys. Chem. A 2021, 125, 9115–9127

reliable that upper-state levels involving mode 24 can be identified by SVLE.

It thus follows that of the five features between 340 and 450 cm^{-1}, only those at 376, 390, and 406 cm^{-1} can be attributed with confidence to PEB. We recommend their assignment as 27_0^2, $26_0^1 28_0^1$, and 15_0^1, respectively, but a different permutation may be valid, depending on the extent of anharmonic coupling among the three D_1 levels. There is little doubt, as for the nearest analogue ($6a_0^1$) in benzyl[53] and phenylacetylene,[69] that a significant Herzberg−Teller moment causes 15_0^1 to be much stronger than FC would impute. The dominant contribution to the (linear) Herzberg−Teller moment for the fundamental transition $1_a' \leftarrow 0''$ of a totally symmetric mode a that is HT-active and only very weakly FC-active can be expressed as

$$\boldsymbol{\mu}_{1_a' \leftarrow 0''}(\mathrm{HT}) = \frac{\partial \boldsymbol{\mu}}{\partial Q_a} \langle 1_a' | Q_a | 0_a'' \rangle \prod_{i \neq a}^{3N-6} \langle 0_i' | 0_i'' \rangle$$

where Duschinsky rotation has been ignored in the product term. The coordinate Q_{15} is subject to a very modest displacement upon excitation; it undergoes negligible Duschinsky rotation ($J_{15'',15'} = 0.998$), and the calculated D_0 and D_1 mode 15 frequencies differ by less than 1.5%. To an excellent approximation, one may thus evaluate the HT integral for mode 15 using vibrational wavefunctions of the same electronic state. The result, of course, is the harmonic oscillator transition moment

$$\langle 1_a' | Q_a | 0_a'' \rangle \approx \langle 1_a'' | Q_a | 0_a'' \rangle = \sqrt{\frac{1}{2 m_a \omega_a}}$$

where m_a and ω_a are the reduced mass and frequency of the ath mode in atomic units. The electronic transition moment gradient $\partial \boldsymbol{\mu}/\partial Q_a$ is calculated by differentiation of the TDB3LYP transition moment function $\mu_z(Q_a)$ (Supporting Information, Figure S2), and the product of zero-level overlap integrals (0.63) is taken from the FCLab II FC calculation. For 15_0^1, we find that $\mu(\mathrm{HT})/\mu(\mathrm{FC}) \sim 12.5$, yielding a roughly 150-fold enhancement in oscillator strength and amounting to about 9% of the 0_0^0 intensity. The experimental intensity ratio $I(15_0^1)/I(0_0^0)$ (whichever of 376, 390, or 406 cm^{-1} one assigns as 15_0^1) is ∼6%; given that the FCHT "15_0^1" intensity is probably diluted by Fermi resonance, our simple calculation appears to be at least qualitatively consistent with observation.

The FC intensities of 27_0^2 and $26_0^1 28_0^1$ are significantly over- and underestimated, respectively. The unscaled B3LYP frequencies give $\sqrt{\nu_{27}''/\nu_{27}'} = 1.06$, which ordinarily would yield an almost negligible 27_0^2 FCF. The calculated strength of 27_0^2, as shown in Figure 2, derives almost entirely from its "24_0^2" character (in terms of the D_0 basis), caused by a substantial predicted Duschinsky rotation (∼15°). However, ν_{24}' is clearly spuriously low, probably by a factor of 2 or more, and the rotation angle concomitantly is too large. We thus contend that 27_0^2 owes most of its intensity to Fermi resonance with 15_0^1. For $26_0^1 28_0^1$, the same kind of resonance is possible but need not be operative for the observed strength to be rationalized. Smith[78] used perturbation theory to derive an expression for the ratio $I(X_0^1 Y_0^1)/I(0_0^0)$ for Duschinsky-mixed nontotally symmetric modes X and Y, in terms of their ground- and excited-state frequencies and the rotational angle θ for Q_X and Q_Y. The expression contains $\cos\theta \sin\theta$ as a multiplicative factor, causing a sensitive angular dependence. The intensity of $X_0^1 Y_0^1$ also increases when the two modes have widely disparate ground-state frequencies that become more similar upon excitation (the mixed vinyl torsion/out-of-plane bend transitions of styrene presenting a classic example[79,80]). Using the B3LYP results directly (i.e., unscaled mode 26 and 28 frequencies and $\theta \sim 3.8°$, neglecting other modes), we calculate $I(X_0^1 Y_0^1)/I(0_0^0) \approx 0.014$. If instead using frequencies derived from our assignments ($\nu_{26}' \sim 320$ and $\nu_{28}' \sim 70$, assuming no anharmonic cross-term), the intensity grows by almost 60%; and further, if θ is increased a mere 2.7°, we find $I(X_0^1 Y_0^1)/I(0_0^0) \approx 0.066$, which essentially agrees with observation for the 390 cm^{-1} band.

These arguments support the identification of 27_0^2, $26_0^1 28_0^1$, and 15_0^1. Concerning their specific assignments, we submit the following. The most reliably calculated harmonic band position (being that of an a_1 mode) is 15_0^1 (406 cm^{-1}, after scaling by 0.976). It will be modestly depressed by vibronic mixing with the bright 2^2B_1 state, but modestly pushed up by Fermi resonance if it is the higher of the uncoupled levels. Its assignment as the highest of the three transitions, at 406 cm^{-1}, is therefore not unreasonable. Its resonance partner, 27_0^2, is assigned at 376 cm^{-1}. The intensity of $26_0^1 28_0^1$ can be well enough explained without invoking anharmonic coupling, and the assignment $26_0^1 28_0^1$ = 390 cm^{-1} provides better agreement with theory for mode 26. The levels 15^1 and 27^2 are approximately equally bright and separated by 30 cm^{-1}, consistent with $V \sim 15$ cm^{-1} and $\Delta E \sim 0.5$ cm^{-1} or smaller. Other types of resonance are possible (e.g., $27_0^2/26_0^1 28_0^1$, requiring a quartic potential term) but probably less important. SVLE spectroscopy should provide a rigorous test of our arguments.

The harmonic frequencies $\nu_{26} = 320$ cm^{-1} and $\nu_{27} \sim 195$ cm^{-1} (in zero order) deriving from the above assignments should give rise to overtones and combinations close to observed features −641 cm^{-1}, assigned as 26_0^2, and 648 cm^{-1}, assigned as $25_0^1 27_0^1$—, lending some credence to our analysis. Both assignments are tentative, however. The 641 cm^{-1} feature is much weaker in fluorescence (Supporting Information, Figure S4), suggesting an overlapping transition of another isomer. We would expect 26_0^2 to be weak (1−2% of the origin) on FC premises, and similarly for $25_0^1 27_0^1$, unless modes 25 and 27 undergo greater rotation (of order 10° using the theory of Smith,[78] instead of the predicted 5°). If one nevertheless accepts that 648 cm^{-1} = $25_0^1 27_0^1$, it follows that $\nu_{25}' \approx 450$ cm^{-1}, and consequently that 25_0^2 might be expected near 900 cm^{-1}, leading us to tentatively assign 887 cm^{-1} = 25_0^2.

Like 15_0^1, 14_0^1 (assigned at 693 cm^{-1}) is much stronger than the FC prediction, again because of a considerable Herzberg−Teller moment. Using the procedure described above for 15_0^1, we calculate $I(14_0^1)/I(0_0^0) \sim 0.24$, which is within a factor of roughly two of observation (0.12). The bands at 698 and 788 cm^{-1} are assigned as 19_0^2 and 18_0^2, respectively. Neither transition should be strong in zero order, but both are close to a_1 fundamentals. In particular, there can be little doubt that 18_0^2, being the third-strongest band in the spectrum, owes most of its intensity to a resonance with 13_0^1. The feature at 740 cm^{-1} lies almost halfway between 19_0^2 and 18_0^2, suggesting its assignment as $18_0^1 19_0^1$. However, there is no obvious bright a_1 resonance partner for this band (certainly not within 40 cm^{-1}); if it is not anharmonic mixing (or, less likely, a second-order HT moment) that permits the appearance of $18_0^1 19_0^1$, Duschinsky rotation must be invoked. Indeed, a considerable and essentially mutual rotation of Q_{19} and Q_{18} is predicted ($J_{18''19'}^2 \sim J_{19''18'}^2 \sim 0.35$; $\theta \approx 36°$), which would cause $18_0^1 19_0^1$ to

https://doi.org/10.1021/acs.jpca.1c07039
J. Phys. Chem. A 2021, 125, 9115−9127

overshadow both 19_0^2 and 18_0^2 in the absence of anharmonic coupling.

In the region 900−1250 cm^{-1}, where only three significant transitions are expected (the a_1 fundamentals 12_0^1, 11_0^1, and 10_0^1), three pairs of transitions are observed (recall that the 1245 cm^{-1} band is much too broad to comprise a single transition). This, again, is the calling card of Fermi resonance. The optimal scaling factor (obs./calc.) from all frequencies thus far determined is roughly 0.97, where harmonic frequencies for anharmonically coupled modes are derived from the midpoints of their putative Fermi doublets. Given ν''_{26} = 320 cm^{-1}, we predict that $23^1 26^1 \sim 950$ cm^{-1} and $20^1 26^1 \sim 1250$ cm^{-1}—in close proximity to harmonic predictions for 12^1 and 10^1, respectively, and thus plausibly serving as their resonance partners provided that terms containing $Q_{12}Q_{23}Q_{26}$ and $Q_{10}Q_{20}Q_{26}$ contribute to the potential. Similarly, a likely beneficiary of the oscillator strength carried by 11^1 is 39^2, which lies only 18 cm^{-1} distant in zero order. Modes 11 and 39 both involve in-plane deformations of the phenyl ring, so it is conceivable that motion in one coordinate modulates the potential for the other (giving rise to a term of the form $Q_{11}Q_{39}^2$). We will know how valid these assignments are once the corresponding ground-state levels have been observed.

Perhaps the highest feature to admit a meaningful zero-order assignment is 9_0^1, which involves substantial CH-bending character and is unsurprisingly weak. At energies above 1400 cm^{-1}, there is a rapidly mounting density of possible a_1 combinations built onto the 788−791 false origins, potentially causing several accidental degeneracies with fundamentals for modes 8−6. In addition, the D_1 lifetime in this region becomes comparable to the laser pulse duration, perhaps due to an onset of non-radiative relaxation pathways, rendering R2C2PI detection difficult and intensities consequently enigmatic. This is at least part of the reason that modes 6 and 5—the quinoidal distortion and acetylenic stretch—are apparently weak, though FC would dictate otherwise (5_0^1 is expected near 2000 cm^{-1}, but surveys to higher energy reveal no additional strong features). Another cause could be that the FC and HT moments interfere destructively because of large negative transition moment gradients (Figure S2), which would yield anomalously large intensities in zero-point fluorescence due to constructive interference.[81,82] The extraction of meaningful vibronic assignments from SVLE in this region is likely to be complicated by intramolecular vibrational redistribution (IVR).[38]

4.4. Other C_9H_7 Isomers. By scanning the time delay between the resonant and ionizing photons while monitoring the R2C2PI signal at the PEB origin wavelength, a D_1 lifetime of order 50−100 ns was inferred for PEB. As such, decay of the PEB excited-state population is substantially complete within about 200 ns of optical excitation. The R2C2PI spectrum recorded with the ionizing photon delivered 200 ns after the optical photon is thus dominated by transitions arising from jet-cooled C_9H_7 discharge products with excited-state lifetimes significantly longer than that of PEB. It becomes clear from the delayed ionization scan (Figure 6) that at least two other isomers contribute to the C_9H_7 R2C2PI spectrum in the region 19,500−20,300 cm^{-1}. The carrier of the 19,948 cm^{-1} band is estimated to have an upper-state lifetime of several μs on the basis of delayed ionization measurements, consistent with an at least 10-fold smaller f-value than that of PEB (f = 0.01), and therefore not inconsistent with MEB (f = 0.0001). The discharge conditions were optimized in favor of the 19,948

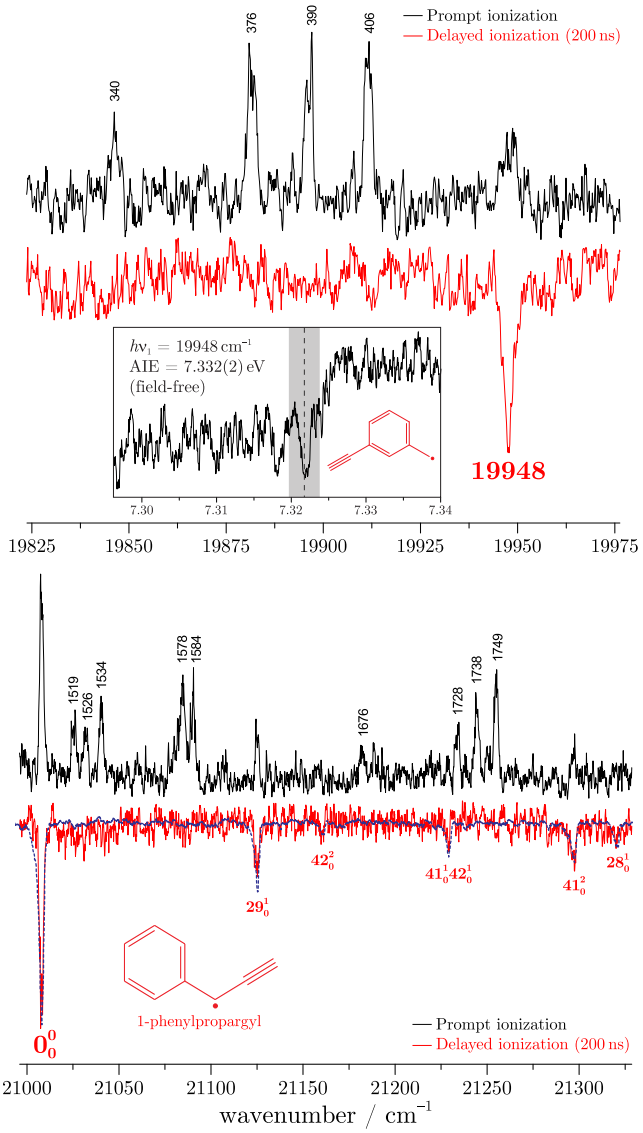

Figure 6. Comparison of R2C2PI spectra recorded with delays of 5 ns (black) and 200 ns (red, reflected) between the resonant and ionizing photons. The carrier of the 19,948 cm^{-1} feature is identified as MEB by a two-color ion-yield scan (inset, top panel); in the bottom panel, the presence of 1PP is confirmed by comparison with the previously reported[37] R2C2PI spectrum (dashed blue trace).

cm^{-1} feature, and a two-color ion-yield curve was recorded, exposing a clear 2CAP threshold near 7.332 eV, within 0.05 eV of both B3LYP and CBS-QB3 predictions of the MEB AIE. We have not yet undertaken R2C2PI experiments using *m*-ethynyltoluene (presumably the best precursor for MEB), but a preliminary LIF survey of the *m*-ethynyltoluene discharge is dominated by a band at 19,948 cm^{-1}. No reproducible features attributable to this species have yet been observed further to the red, implying 19,948 cm^{-1} is the MEB D_0−D_1 origin. The computed vertical f-values of PEB (0.01) and 1PP (0.02) are similar, but the former has a greatly diminished D_1 lifetime near the 1PP D_0−D_1 origin (21,007 cm^{-1}). The optical spectrum of 1PP has been studied by one of us in detail;[37,38] the delayed ionization scan (Figure 6, red trace, lower panel) is essentially congruent with the previously reported 1PP R2C2PI spectrum (overlain dashed blue trace).

https://doi.org/10.1021/acs.jpca.1c07039
J. Phys. Chem. A 2021, 125, 9115−9127

Analysis of the precursor (*p*-ethynyltoluene, Sigma-Aldrich) by ^{1}H NMR indicates a purity of least 99.5% (Supporting Information, Section S5). The seed ratio of *p*-ethynyltoluene delivered to the pulsed nozzle was 0.05−0.1%. During R2C2PI scans, no discharge products were observed in the mass spectrum, resonantly or non-resonantly, for $m/z > 116$ ($m/z = 116$ being the precursor, observed by UV multi-photon ionization). Unless the computed oscillator strengths for PEB, MEB, and 1PP are inaccurate by at least 2 orders of magnitude—which the D_1 lifetime data suggest is not the case (Table 5)—MEB and 1PP are both produced in the discharge

Table 5. Observed Relative Origin Band Intensities (from Figure 2), Calculated Vertical D_0−D_1 Oscillator Strengths (f), and Observed Upper-State Lifetimes of PEB, MEB, and 1PP Radicals[a]

	PEB	MEB	1PP
0_0^0 intensity (rel.)	1	0.03	0.15
f (calc.)	0.01	0.0001	0.02
D_1 lifetime (0^0 level)	50−100 ns[b]	>1 μs[b]	250 ns[38]
precursor abundance	>99.5%	<0.3%	none detected

[a]"Precursor abundance" refers to the abundance (Supporting Information, Section S5) in the C_9H_8 sample of the optimal precursor for each radical: *p*-ethynyltoluene (for PEB); *m*-ethynyltoluene (for MEB); and 3-phenyl-1-propyne (for 1PP). [b]Estimated by scanning the time delay between resonant and ionizing photons in R2C2PI.

in vastly higher abundances than can be explained by sample impurities. Because bimolecular hydrocarbon chemistry appears to have been largely inoperative in the expansion, the three radicals must be connected by somewhat facile unimolecular rearrangement pathways.

During a recent spectroscopic interrogation of a dilute toluene discharge,[45] the coexistence of *o*-, *m*-, *p*-xylyl (methylbenzyl) radicals (C_8H_9) in the expansion was established by R2C2PI in the region 480−450 nm. In the same work, rearrangement of xylyl radicals in discharges of the parent xylenes was also observed spectroscopically, consistent with earlier VUV-PIMS flash pyrolysis work using xylylbromide precursors.[54,83] The spectrum of a previously unreported C_8H_9 product was observed near 385 nm under the same experimental conditions and attributed to the methyltropyl radical. High-quality calculations of part of the C_8H_9 PES strongly supported the assertion that interconversion of xylyl radicals proceeds *via* the methyltropyl intermediate. It is not unreasonable to speculate that a similar species—ethynyltropyl radical—could connect the ethynylbenzyl isomers (1PP may also be called α-ethynylbenzyl). In future experiments, using the appropriate top-down precursors, we hope to study MEB in further detail, firmly identify the ortho isomer (perhaps the carrier of the 340 cm^{-1} feature), and survey the near-UV for evidence of a putative ethynyltropyl intermediate.

5. CONCLUSIONS

The resonance-stabilized PEB radical has been spectroscopically identified under jet-cooled conditions using resonant two-photon ionization. A FC simulation of the $D_0(^2B_1)$−$D_1(^2B_1)$ transition using geometries and harmonic frequencies from B3LYP/TDB3LYP calculations is sufficiently informative that several FC-active a_1 modes, and a few nontotally symmetric modes, can be assigned readily. However, the intensities of many features can only be rationalized if the influences of Herzberg−Teller coupling and more importantly Fermi resonance are taken into account. The former effect causes enhancement for some a_1 modes by intensity-borrowing from a much brighter, higher-lying B_1 state, similar to the well-known case of the totally symmetric 6*a* mode of benzyl.[53,66] The latter effect gives rise to closely spaced doublets of comparable intensity in almost every instance where a lone a_1 fundamental is expected. Plausible assignments for the resonance partners have been suggested; it should be possible to confirm our analyses using insights from SVLE measurements that are presently being undertaken in our laboratory. Other C_9H_7 isomers were also observed in the R2C2PI spectrum: we have conclusively identified the meta species, with a putative origin at 19,948 cm^{-1}; a feature at 19,846 cm^{-1} that cannot be reasonably assigned to PEB may belong to the ortho isomer; and the known D_0−D_1 transition of 1PP is quite conspicuous. The simultaneous presence of these radicals in a dilute *p*-ethynyltoluene discharge almost certainly cannot be explained by sample impurities or bimolecular processes involving smaller species, pointing to the existence of feasible unimolecular rearrangement pathways. By analogy with the C_8H_9 surface, whereby the methyltropyl radical is a likely nexus for interconversion of methylbenzyl radicals observed in discharges of toluene and its derivatives,[45] we posit that the yet unidentified ethynyltropyl radical might be detectable in coexistence with the ethynylbenzyl radicals. R2C2PI assays for this species in the near-UV are planned.

■ ASSOCIATED CONTENT

Supporting Information

The Supporting Information is available free of charge at https://pubs.acs.org/doi/10.1021/acs.jpca.1c07039.

Frontier orbitals; TDB3LYP transition moment functions for a_1 modes; a_2 and b_1 Duschinsky matrices; comparison of R2C2PI and LIF spectra; ^{1}H NMR analysis of the *p*-ethynyltoluene sample used in experiments; optimized Cartesian coordinates of D_0 and D_1 states of PEB; and selected normal mode displacement vectors for PEB (PDF)

■ AUTHOR INFORMATION

Corresponding Author

Neil J. Reilly − *Department of Chemistry, University of Massachusetts Boston, Boston, Massachusetts 02125, United States*; orcid.org/0000-0001-5572-4784; Email: neil.reilly@umb.edu

Authors

Sederra D. Ross − *Department of Chemistry, University of Massachusetts Boston, Boston, Massachusetts 02125, United States*

Jonathan Flores − *Department of Chemistry, University of Massachusetts Boston, Boston, Massachusetts 02125, United States*

Sima Khani − *Department of Chemistry, University of Massachusetts Boston, Boston, Massachusetts 02125, United States*

Daniel M. Hewett − *Department of Chemistry, University of Massachusetts Boston, Boston, Massachusetts 02125, United States*

Complete contact information is available at: https://pubs.acs.org/10.1021/acs.jpca.1c07039

Notes

The authors declare no competing financial interest.

■ ACKNOWLEDGMENTS

This research was supported by awards from the US National Science Foundation (grant no. CHE: 1665341) and the American Chemical Society Petroleum Research Fund (Doctoral New Investigator grant no. 57533-DNI6). S.D.R. acknowledges the US National Science Foundation for a Graduate Research Fellowship. J.F. thanks Oracle for fellowship support during this project.

■ REFERENCES

(1) Buckingham, G. T.; Porterfield, J. P.; Kostko, O.; Troy, T. P.; Ahmed, M.; Robichaud, D. J.; Nimlos, M. R.; Daily, J. W.; Ellison, G. B. The Thermal Decomposition of the Benzyl Radical in a Heated Micro-reactor. II. Pyrolysis of the Tropyl Radical. *J. Chem. Phys.* **2016**, *145*, 14305.

(2) Buckingham, G. T.; Ormond, T. K.; Porterfield, J. P.; Hemberger, P.; Kostko, O.; Ahmed, M.; Robichaud, D. J.; Nimlos, M. R.; Daily, J. W.; Ellison, G. B. The Thermal Decomposition of the Benzyl Radical in a Heated Micro-Reactor. I. Experimental Findings. *J. Chem. Phys.* **2015**, *142*, 44307.

(3) da Silva, G.; Cole, J. A.; Bozzelli, J. W. Thermal Decomposition of the Benzyl Radical to Fulvenallene (C_7H_6) + H. *J. Phys. Chem. A* **2009**, *113*, 6111−6120.

(4) McEnally, C. S.; Pfefferle, L. D.; Atakan, B.; Kohse-Höinghaus, K. Studies of Aromatic Hydrocarbon Formation Mechanisms in Flames: Progress Towards Closing the Fuel Gap. *Prog. Energy Combust.* **2006**, *32*, 247−294.

(5) Miller, J. A.; Melius, C. F. Kinetic and Thermodynamic Issues in Formation of Aromatic Compounds in Flames of Aliphatic Fuels. *Combust. Flame* **1992**, *91*, 21−39.

(6) Miller, J. A.; Klippenstein, S. J. The Recombination of Propargyl Radicals and Other Reactions on aC_6H_6 Potential. *J. Phys. Chem. A* **2003**, *107*, 7783−7799.

(7) Richter, H.; Howard, J. B. Formation and Consumption of Single-Ring Aromatic Hydrocarbons and Their Precursors in Premixed Acetylene, Ethylene and Benzene Flames. *Phys. Chem. Chem. Phys.* **2002**, *4*, 2038−2055.

(8) Melius, C. F.; Colvin, M. E.; Marinov, N. M.; Pit, W. J.; Senkan, S. M. Reaction Mechanisms in Aromatic Hydrocarbon Formation Involving the C_5H_5 Cyclopentadienyl Moiety. *Proc. Combust. Inst.* **1996**, *26*, 685−692.

(9) Long, A. E.; Merchant, S. S.; Vandeputte, A. G.; Carstensen, H.-H.; Vervust, A. J.; Marin, G. B.; Van Geem, K. M.; Green, W. H. Pressure Dependent Kinetic Analysis of Pathways to Naphthalene from Cyclopentadienyl Recombination. *Combust. Flame* **2018**, *187*, 247−256.

(10) Mebel, A. M.; Landera, A.; Kaiser, R. I. Formation Mechanisms of Naphthalene and Indene: From the Interstellar Medium to Combustion Flames. *J. Phys. Chem. A* **2017**, *121*, 901−926.

(11) Matsugi, A.; Miyoshi, A. Computational study on the recombination reaction between benzyl and propargyl radicals. *Int. J. Chem. Kinet.* **2012**, *44*, 206−218.

(12) Colket, M. B.; Seery, D. J. Reaction Mechanisms for Toluene Pyrolysis. *Proc. Combust. Inst.* **1994**, *25*, 883−891.

(13) Johansson, K. O.; Head-Gordon, M. P.; Schrader, P. E.; Wilson, K. R.; Michelsen, H. A. Resonance-stabilized Hydrocarbon-Radical Chain Reactions May Explain Soot Inception and Growth. *Science* **2018**, *361*, 997−1000.

(14) Thapa, J.; Spencer, M.; Akhmedov, N. G.; Goulay, F. Kinetics of the OH Radical Reaction with Fulvenallene from 298 to 450 K. *J. Phys. Chem. Lett.* **2015**, *6*, 4997−5001.

(15) Abhinavam Kailasanathan, R. K.; Thapa, J.; Goulay, F. Kinetic Study of the OH Radical Reaction with Phenylacetylene. *J. Phys. Chem. A* **2014**, *118*, 7732−7741.

(16) Allodi, M. A.; Kirschner, K. N.; Shields, G. C. Thermodynamics of the Hydroxyl Radical Addition to Isoprene. *J. Phys. Chem. A* **2008**, *112*, 7064−7071.

(17) Cherchneff, I.; Barker, J. R.; Tielens, A. G. G. M. Polycyclic Aromatic Hydrocarbon Formation in Carbon-Rich Stellar Envelopes. *Astrophys. J.* **1992**, *401*, 269−287.

(18) Cherchneff, I. The Formation of Polycyclic Aromatic Hydrocarbons in Evolved Circumstellar Environments. *EAS Publ. Ser.* **2011**, *46*, 177−189.

(19) Zhao, L.; Lu, W.; Ahmed, M.; Zagidullin, M. V.; Azyazov, V. N.; Morozov, A. N.; Mebel, A. M.; Kaiser, R. I. Gas-phase Synthesis of Benzene Via the Propargyl Radical Self-reaction. *Sci. Adv.* **2021**, *7*, No. eabf0360.

(20) Loison, J. C.; Dobrijevic, M.; Hickson, K. M. The Photochemical Production of Aromatics in the Atmosphere of Titan. *Icarus* **2019**, *329*, 55−71.

(21) Polino, D.; Parrinello, M. Combustion Chemistry via Metadynamics: Benzyl Decomposition Revisited. *J. Phys. Chem. A* **2015**, *119*, 978−989.

(22) Dinadayalane, T. C.; Priyakumar, U. D.; Sastry, G. N. Exploration of C_6H_6 Potential Energy Surface: A Computational Effort to Unravel the Relative Stabilities and Synthetic Feasibility of New Benzene Isomers. *J. Phys. Chem. A* **2004**, *108*, 11433−11448.

(23) The C_6H_6 surface, for instance, has been suggested to host as many as 200 stable minima, of which more than 80 may lie within ca. 400 kJ mol^{-1} of ground.[22]

(24) Fischer, K. H.; Herterich, J.; Fischer, I.; Jaeqx, S.; Rijs, A. M. Phenylpropargyl Radicals and Their Dimerization Products: An IR/UV Double Resonance Study. *J. Phys. Chem. A* **2012**, *116*, 8515−8522.

(25) Hirsch, F.; Flock, M.; Fischer, I.; Bakels, S.; Rijs, A. M. The Gas-Phase Infrared Spectra of Xylyl Radicals. *J. Phys. Chem. A* **2019**, *123*, 9573−9578.

(26) Krechkivska, O.; Wilcox, C.; O'Connor, G. D.; Nauta, K.; Kable, S. H.; Schmidt, T. W. Ionization Energies of Three Resonance-Stabilized Radicals: Cyclohexadienyl (d_n, n = 0, 1, 6, 7), 1-Phenylpropargyl, and Methylcyclohexadienyl. *J. Phys. Chem. A* **2014**, *118*, 10252−10258.

(27) Schmidt, T. W. The Electronic Spectroscopy of Resonance-Stabilised Hydrocarbon Radicals. *Int. Rev. Phys. Chem.* **2016**, *35*, 209−242.

(28) Reilly, N. J.; Kokkin, D. L.; Ward, M. L.; Flores, J.; Ross, S. D.; McCaslin, L. M.; Stanton, J. F. Gas-Phase Optical Detection of 3-Ethynylcyclopentenyl: A Resonance-Stabilized C_7H_7 Radical with an Embedded 1-Vinylpropargyl Chromophore. *J. Am. Chem. Soc.* **2020**, *142*, 10400−10411.

(29) Ross, S. D.; Flores, J.; Hewett, D. M.; Reilly, N. J. Electronic Spectroscopy of cis- and trans-meta-Vinylbenzyl Radicals. *J. Phys. Chem. A* **2021**, *125*, 6420−6436.

(30) Zhang, T.; Zhang, L.; Hong, X.; Zhang, K.; Qi, F.; Law, C. K.; Ye, T.; Zhao, P.; Chen, Y. An Experimental and Theoretical Study of Toluene Pyrolysis with Tunable Synchrotron Vuv Photoionization and Molecular-beam Mass Spectrometry. *Combust. Flame* **2009**, *156*, 2071−2083.

(31) Yuan, W.; Li, Y.; Dagaut, P.; Yang, J.; Qi, F. Investigation on the Pyrolysis and Oxidation of Toluene Over a Wide Range Conditions. I. Flow Reactor Pyrolysis and Jet Stirred Reactor Oxidation. *Combust. Flame* **2015**, *162*, 3−21.

(32) Li, Y.; Zhang, L.; Yuan, T.; Zhang, K.; Yang, J.; Yang, B.; Qi, F.; Law, C. K. Investigation on Fuel-rich Premixed Flames of Monocyclic Aromatic Hydrocarbons: Part I. Intermediate Identification and Mass Spectrometric Analysis. *Combust. Flame* **2010**, *157*, 143−154.

(33) Hemberger, P.; Steinbauer, M.; Schneider, M.; Fischer, I.; Johnson, M.; Bodi, A.; Gerber, T. Photoionization of Three Isomers of the C_9H_7 Radical. *J. Phys. Chem. A* **2010**, *114*, 4698−4703.

(34) Kim, J. B.; Weichman, M. L.; Yacovitch, T. I.; Shih, C.; Neumark, D. M. Slow Photoelectron Velocity-Map Imaging Spectroscopy of the C_9H_7 (Indenyl) and $C_{13}H_9$ (Fluorenyl) Anions. *J. Chem. Phys.* **2013**, *139*, 104301.

https://doi.org/10.1021/acs.jpca.1c07039
J. Phys. Chem. A 2021, 125, 9115−9127

(35) Kumar, A.; Agrawal, S.; Rao, T. R.; Sarkar, R. Rationalization of Photo-detachment Spectra of the Indenyl Anion (C_9H_7) from the Perspective of Vibronic Coupling Theory. *Phys. Chem. Chem. Phys.* **2019**, *21*, 22359−22376.
(36) Izumida, T.; Inoue, K.; Noda, S.; Yoshida, H. Electronic Spectra of Some Aromatic Free Radicals. *Bull. Chem. Soc. Jpn.* **1981**, *54*, 2517−2518.
(37) Reilly, N. J.; Kokkin, D. L.; Nakajima, M.; Nauta, K.; Kable, S. H.; Schmidt, T. W. Spectroscopic Observation of the Resonance-Stabilized 1-Phenylpropargyl Radical. *J. Am. Chem. Soc.* **2008**, *130*, 3137−3142.
(38) Reilly, N. J.; Nakajima, M.; Troy, T. P.; Chalyavi, N.; Duncan, K. A.; Nauta, K.; Kable, S. H.; Schmidt, T. W. Spectroscopic Identification of the Resonance-Stabilized cis- and trans-1-vinyl-propargyl Radicals. *J. Am. Chem. Soc.* **2009**, *131*, 13423−13429.
(39) O'Connor, G. D.; Woodhouse, G. V.; Troy, T. P.; Schmidt, T. W. Double-resonance Spectroscopy of Radicals: Higher Electronic Excited States of 1- and 2-naphthylmethyl, 1-phenylpropargyl and 9-anthracenylmethyl. *Mol. Phys.* **2015**, *113*, 2138−2147.
(40) Troy, T. P.; Chalyavi, N.; Menon, A. S.; O'Connor, G. D.; Fückel, B.; Nauta, K.; Radom, L.; Schmidt, T. W. The Spectroscopy and Thermochemistry of Phenylallyl Radical Chromophores. *Chem. Sci.* **2011**, *2*, 1755−1765.
(41) Holzmeier, F.; Lang, M.; Hemberger, P.; Fischer, I. Improved Ionization Energies for the Two Isomers of Phenylpropargyl Radical. *ChemPhysChem* **2014**, *15*, 3489−3492.
(42) Matsugi, A.; Miyoshi, A. Reactions of o-benzyne with Propargyl and Benzyl Radicals: Potential Sources of Polycyclic Aromatic Hydrocarbons in Combustion. *Phys. Chem. Chem. Phys.* **2012**, *14*, 9722−9728.
(43) M06-2x/6-311+G(3df,2p)//B3LYP/6-311G(d,p) calculations (ref 42) indicate that 1PP/3PP lie 134/138 kJ mol^{-1} above indenyl; our own calculations (B3LYP/6-311++G(d,p) and CBS-QB3) suggest PEB lies roughly 20 kJ mol^{-1} above 1PP. The same calculations indicate MEB and OEB are less stable than PEB by roughly 8 and 4 kJ mol^{-1}, respectively. Uncertainties are of order 10 kJ mol^{-1}.
(44) Hamon, S.; Le Picard, S. D.; Canosa, A.; Rowe, B. R.; Smith, I. W. M. Low Temperature Measurements of the Rate of Association to Benzene Dimers in Helium. *J. Chem. Phys.* **2000**, *112*, 4506−4516.
(45) Reilly, N. J.; da Silva, G.; Wilcox, C. M.; Ge, Z.; Kokkin, D. L.; Troy, T. P.; Nauta, K.; Kable, S. H.; McCarthy, M. C.; Schmidt, T. W. Interconversion of Methyltropyl and Xylyl Radicals: A Pathway Unavailable to the Benzyl−Tropyl Rearrangement. *J. Phys. Chem. A* **2018**, *122*, 1261−1269.
(46) In the same way, for instance, that the xylyl radicals can be produced by CH addition to toluene.[45]
(47) Detection of emission from the D1 zero-point level of ortho-ethynylbenzyl has been claimed (*Chem. Phys. Lett.*, 2018, 712, 139−143), but close inspection of the reported spectrum reveals that essentially every significant molecular feature can be assigned to either 1-indanyl or 1-phenylpropargyl with high confidence.
(48) Fukushima, M.; Saito, K.; Obi, K. Jet Spectroscopy of the D_1 2^2B_1 − D_0 1^2B_1 Transition of the p-Cyanobenzyl Radical. *J. Mol. Spectrosc.* **1996**, *180*, 389−397.
(49) Lee, S. K.; Ahn, B. U. Vibronic Spectroscopy of Jet-cooled p-cyanobenzyl Radical: $D_1 \rightarrow D_0$ Spectra and Vibrational Mode Assignments. *Chem. Phys. Lett.* **2000**, *320*, 601−606.
(50) Lee, S. K.; Kim, Y. N. Vibronic Spectroscopy of Benzyl-Type Radicals: Jet-Cooled m-Cyanobenzyl Radical in the $D_1 \rightarrow D_0$ Transition. *J. Phys. Chem. A* **2004**, *108*, 3727−3731.
(51) Lee, S. K.; Chae, S. Y. Vibronic Emission Spectroscopy of the Jet-Cooled o-Chlorobenzyl Radical in the $D_1 \rightarrow D_0$ Transition. *J. Phys. Chem. A* **2002**, *106*, 8054−8058.
(52) Negri, F.; Orlandi, G.; Zerbetto, F.; Zgierski, M. Z. Quantum Chemical and Vibronic Analysis of the $1^2B_2 \leftrightarrow 1^2A_2$, 2^2B_2 Transition in Benzyl-H_7 and Benzyl-D_7 Radicals. *J. Chem. Phys.* **1990**, *93*, 600−608.
(53) Eiden, G. C.; Weisshaar, J. C. Vibronic Coupling Mechanism in the A^2A_2−BB^2B_2Excited States of Benzyl Radical. *J. Chem. Phys.* **1996**, *104*, 8896−8912.
(54) Hemberger, P.; Trevitt, A. J.; Gerber, T.; Ross, E.; da Silva, G. Isomer-Specific Product Detection of Gas-Phase Xylyl Radical Rearrangement and Decomposition Using VUV Synchrotron Photoionization. *J. Phys. Chem. A* **2014**, *118*, 3593−3604.
(55) Thaddeus, P.; McCarthy, M. C. Carbon Chains and Rings in the Laboratory and in Space. *Spectrochim. Acta, Part A* **2001**, *57*, 757−774.
(56) Frisch, M. J.; Trucks, G. W.; Schlegel, H. B.; Scuseria, G. E.; Robb, M. A.; Cheeseman, J. R.; Scalmani, G.; Barone, V.; Mennucci, B.; Petersson, G. A.; et al. *Gaussian 09*, Revision A.1.; Gaussian Inc.: Wallingford CT, 2009.
(57) Pugliesi, I.; Müller-Dethlefs, K. The Use of Multidimensional Franck-Condon Simulations to Assess Model Chemistries: A Case Study on Phenol. *J. Phys. Chem. A* **2006**, *110*, 4657−4667. http://www.fclab2.net/index.html A free download of the software can be found at
(58) Pugliesi, I.; Tonge, N. M.; Hornsby, K. E.; Cockett, M. C. R.; Watkins, M. J. An Examination of Structural Characteristics of Phenylacetylene by Vibronic and Rovibronic Simulations of ab initio Data. *Phys. Chem. Chem. Phys.* **2007**, *9*, 5436−5445.
(59) Western, C. M. Pgopher: A Program for Simulating Rotational, Vibrational and Electronic Spectra. *J. Quant. Spectrosc. Radiat. Transfer* **2017**, *186*, 221−242.
(60) Troy, T. P.; Nakajima, M.; Chalyavi, N.; Clady, R. G. C. R.; Nauta, K.; Kable, S. H.; Schmidt, T. W. Identification of the Jet-Cooled 1-Indanyl Radical by Electronic Spectroscopy. *J. Phys. Chem. A* **2009**, *113*, 10279−10283.
(61) Chalyavi, N.; Troy, T. P.; Nakajima, M.; Gibson, B. A.; Nauta, K.; Sharp, R. G.; Kable, S. H.; Schmidt, T. W. Excitation and Emission Spectra of Jet-Cooled Naphthylmethyl Radicals. *J. Phys. Chem. A* **2011**, *115*, 7959−7965.
(62) Maity, S.; Steglich, M.; Maier, J. P. Electronic Spectroscopy of Resonantly Stabilized Aromatic Radicals: 1-Indanyl and Methyl Substituted Analogues. *J. Phys. Chem. A* **2015**, *119*, 9078−9084.
(63) Makuvaza, J. T.; Loman, J. L.; Kokkin, D. L.; Reid, S. A. Probing Cooperativity in C−H··· N and C−H···π Interactions: Dissociation energies of Aniline$(CH_4)_n$ (n = 1, 2) van der Waals Complexes from Resonant Ionization and Velocity Mapped Ion Imaging Measurements. *J. Chem. Phys.* **2020**, *153*, 044303.
(64) Coulson, C. A.; Rushbrooke, G. S. Note on the Method of Molecular Orbitals. *Math. Proc. Cambridge Philos. Soc.* **1940**, *36*, 193−200.
(65) Longuet-Higgins, H. C.; Pople, J. A. The Electronic Spectra of Aromatic Molecules IV: Excited States of Odd Alternant Hydrocarbon Radicals and Ions. *Proc. Phys. Soc., London, Sect. A* **1955**, *68*, 591−600.
(66) Fukushima, M.; Obi, K. Jet Spectroscopy of Benzyl and Benzyl-α-D_2. *J. Chem. Phys.* **1992**, *96*, 4224−4232.
(67) Fukushima, M.; Obi, K. Jet Spectroscopy and Excited State Dynamics of Benzyl and Substituted Benzyl Radicals. *J. Chem. Phys.* **1990**, *93*, 8488−8497.
(68) Hiratsuka, H.; Mori, K.; Shizuka, H.; Fukushima, M.; Obi, K. Emitting States of Benzyl, p-fluorobenzyl and p-cyanobenzyl Radicals. *Chem. Phys. Lett.* **1989**, *157*, 35−40.
(69) Chang, C.-H.; Lopez, G.; Sears, T. J.; Johnson, P. M. Vibronic Analysis of the S_1 − S_0 Transition of Phenylacetylene Using Photoelectron Imaging and Spectral Intensities Derived from Electronic Structure Calculations. *J. Phys. Chem. A* **2010**, *114*, 8262−8270.
(70) Duschinsky, F. The Importance of the Electron Spectrum in Multi Atomic Molecules. Concerning the Franck-Condon Principle. *Acta Physicochim. URSS* **1937**, *7*, 551−566.
(71) Doktorov, E. V.; Malkin, I. A.; Man'ko, V. I. Dynamical Symmetry of Vibronic Transitions in Polyatomic Molecules and the Franck-Condon Principle. *J. Mol. Spectrosc.* **1977**, *64*, 302−326.

https://doi.org/10.1021/acs.jpca.1c07039
J. Phys. Chem. A 2021, 125, 9115−9127

(72) Knight, A. E. W.; Lawburgh, C. M.; Parmenter, C. S. n, π^* Fluorescence from Selected Vibronic Levels of Pyrimidine Vapor: Franck−condon Factors and Excited State Anharmonic Coupling. *J. Chem. Phys.* **1975**, *63*, 4336−4351.
(73) Knight, A. E. W.; Kable, S. H. The $S_1 - S_0$ ($^1B_{2u} - ^1A_g$) Transition of p-difluorobenzene Cooled in a Supersonic Free Jet Expansion. Excitation and Dispersed Fluorescence Spectra, Vibrational Assignments, Fermi Resonances, and Forbidden Transitions. *J. Chem. Phys.* **1988**, *89*, 7139−7160.
(74) Honjou, H.; Yoshimine, M.; Pacansky, J. Theoretical Studies on the Ground State and Low-Lying Doublet Excited States of the Propargyl Radical. *J. Phys. Chem.* **1987**, *91*, 4455−4459.
(75) Eisfeld, W. Calculation of the Vibrationally Resolved Electronic Absorption Spectrum of the Propargyl Radical (H_2CCCH). *J. Phys. Chem. A* **2006**, *110*, 3903−3910.
(76) Wyss, M.; Riaplov, E.; Maier, J. P. Electronic and Infrared Spectra of $H_2C_3H^+$ and Cyclic $C_3H_3^+$in Neon Matrices. *J. Chem. Phys.* **2001**, *114*, 10355−10361.
(77) Flores, J.; Ward, M. L.; Ross, S. D.; Reilly, N. J. Ionization Energies and Single Vibronic Level Emission (SVLE) Spectroscopy of cis- and trans-1-Vinylpropargyl Radicals. *Presented at the 74th International Symposium on Molecular Spectroscopy*; University of Illinois Urbana-Champaign: USA, 2019. URL: http://hdl.handle.net/2142/104470.
(78) Smith, W. L. Intensities of Transitions in Non-Totally Symmetric Vibrations in the Electronic Spectra of Polyatomic Molecules. *J. Mol. Spectrosc.* **1996**, *176*, 95−98.
(79) Syage, J. A.; Al Adel, F.; Zewail, A. H. Jet-Cooled Styrene: Spectra and Isomerization. *Chem. Phys. Lett.* **1983**, *103*, 15−22.
(80) Mahmoud, H.; Germanenko, I. N.; Ibrahim, Y.; El-Shall, M. S. Resonant Two-Photon Ionization Spectroscopy of Styrene (Methanol)$_n$ Clusters, n = 1 − 9. *J. Phys. Chem. A* **2003**, *107*, 5920−5932.
(81) Craig, D. P.; Small, G. J. Totally Symmetric Vibronic Perturbations and the Phenanthrene 3400Å Spectrum. *J. Chem. Phys.* **1969**, *50*, 3827−3834.
(82) Hohlneicher, G.; Wolf, J. Interference between Franck-Condon and Herzberg-Teller Contributions in Naphthalene and Phenanthrene. *Ber. Bunsenges. Phys. Chem.* **1995**, *99*, 366−369.
(83) Hemberger, P.; Trevitt, A. J.; Ross, E.; da Silva, G. Direct Observation of para-Xylylene as the Decomposition Product of the meta-Xylyl Radical Using VUV Synchrotron Radiation. *J. Phys. Chem. Lett.* **2013**, *4*, 2546−2550.

https://doi.org/10.1021/acs.jpca.1c07039
J. Phys. Chem. A 2021, 125, 9115−9127